

# Assessing Granular Debris-Flow Impact Forces on Bridge Superstructures

Caroline Friedl<sup>1</sup>; Christian Scheidl<sup>2</sup>; Susanna Wernhart<sup>3</sup>; and Dirk Proske<sup>4</sup>

**Abstract:** In countries similar to Austria, bridges fail due to debris-flow impact on a regular basis. As there is a large uncertainty in terms of the acting forces during these events, this study examines debris-flow impact forces on bridge superstructures. We first set up an idealized load pattern for the load case of debris-flow impact on a bridge superstructure. Second, we conducted 60 experiments in a small-scale physical model (scale 1:30), where we measured debris-flow impact forces on six different bridge profiles in the presence and absence of a bridge pier with two 3-axis force sensors installed at the bridge abutments. Our findings indicate that there is an influence of the superstructure profiles on the magnitude of the effective frontal debris-flow impact force while the presence or absence of a bridge pier affects the direction of the effective frontal impact force, but not necessarily its magnitude. Our results also indicate that the effective frontal impact force acts mainly in the horizontal direction as the vertical proportion is mostly <10%. We found that the forces that act on bridge superstructures are on average between one- and three-fifths of the peak debris-flow force. Our findings can contribute to a better design of bridges against debris-flow impact in the future. DOI: [10.1061/JBENF2.BEENG-6439](https://doi.org/10.1061/JBENF2.BEENG-6439). This work is made available under the terms of the Creative Commons Attribution 4.0 International license, <https://creativecommons.org/licenses/by/4.0/>.

**Practical Applications:** A debris flow is a mixture of stones, plant parts, soil and other solids, and water that often causes great damage in mountainous regions, as it can transfer very large forces. When debris flows hit bridges, they are often destroyed. Because debris flows are expected to become more frequent due to climate change and therefore more damage to bridges can be expected in the future, it is necessary to gain a better understanding of the impact process of a debris flow on a bridge. Here, we looked at the forces acting on the deck of the bridge. To this end, we have carried out small-scale experiments and systematically investigated the magnitude of occurring forces and how they are influenced by different shapes of the bridge. We found that it makes a difference which bridge profile is impacted and that usually less than half of the total force of the debris flow acts on the deck of the bridge. Our discoveries can help to better construct bridges against debris-flow impact in the future.

## Introduction

Mountainous regions are characterized by valleys and steep slopes. This distinctive relief landscape determines, on the one hand, the processes of debris flow and, on the other hand, the fact that bridges are an essential element for the settlement structure of today and for an efficient socioeconomic system. Owing to their landscape characteristics, mountainous regions require a high density of bridges to

enable human activities. The Austrian Federal Railways (ÖBB) operates a rail network with a length of around 5,000 km, which includes over 6,500 bridges. This corresponds to a bridge density of more than one bridge per kilometer (OEBB-Infrastruktur AG 2022). In Switzerland, the bridge density is even higher with over 6,000 bridges on a rail network length of around 3,250 km (Proske et al. 2022; SBB AG 2022). Those mountainous regions are usually also the areas where devastating debris flows are frequently observed and thus pose a threat to bridges. Their destruction is a serious problem, as bridges are critical infrastructures and therefore vital for human activities. According to articles in daily newspapers, at least five bridges were destroyed by debris flows in Austria in 2022. Fig. 1 shows a destroyed bridge in Carinthia, Austria.

Debris flows are gravitational mass movements of heterogeneous mixtures of solids (e.g., rocks, soil, debris) and water. Although their composition varies greatly, debris flows are typically characterized by a certain longitudinal structure (Fig. 2): larger, coarser fragments are found at the steep front (head) of the debris flow, while the constitution becomes increasingly fluid as it progresses across the body of the debris flow with finer sediments and a higher water content to form a hyper-concentrated mass of particles in suspension in the tail (Pierson 2020).

The environment for the initiation of a debris flow usually includes an extensive source of available solid material, steeply inclined slopes, and the addition of moisture. There are different mechanisms that can trigger debris flows: heavy rainfall, snowmelt, dam failures, and lake outbursts, but also earthquakes, landslides, and volcanic eruptions (Chiarle et al. 2007; Fan et al. 2019; Iverson

<sup>1</sup>Institute of Mountain Risk Engineering, Dept. of Civil Engineering and Natural Hazards, Univ. of Natural Resources and Life Sciences, Vienna, Peter-Jordan-Straße 82, 1190 Vienna, Austria (corresponding author). ORCID: <https://orcid.org/0000-0003-4030-0393>. Email: caroline.friedl@boku.ac.at

<sup>2</sup>Institute of Mountain Risk Engineering, Dept. of Civil Engineering and Natural Hazards, Univ. of Natural Resources and Life Sciences, Vienna, Peter-Jordan-Straße 82, 1190 Vienna, Austria. ORCID: <https://orcid.org/0000-0002-5625-6238>.

<sup>3</sup>Institute of Mountain Risk Engineering, Dept. of Civil Engineering and Natural Hazards, Univ. of Natural Resources and Life Sciences, Vienna, Peter-Jordan-Straße 82, 1190 Vienna, Austria.

<sup>4</sup>Institute of Mountain Risk Engineering, Dept. of Civil Engineering and Natural Hazards, Univ. of Natural Resources and Life Sciences, Vienna, Peter-Jordan-Straße 82, 1190 Vienna, Austria; School of Architecture, Wood and Civil Engineering, Bern Univ. of Applied Sciences, Pestalozzistraße 20, 3401 Burgdorf, Switzerland.

Note. This manuscript was submitted on April 24, 2023; approved on January 8, 2024; published online on March 27, 2024. Discussion period open until August 27, 2024; separate discussions must be submitted for individual papers. This paper is part of the *Journal of Bridge Engineering*, © ASCE, ISSN 1084-0702.



**Fig. 1.** Bridge after debris-flow impact, Carinthia, Austria 2022. (Image courtesy of Tazio C. Bernardi.)

2000; Mostbauer et al. 2018; Prenner et al. 2019). In the Alpine region, heavy rainfall is considered to be the most frequent cause for triggering debris flows (Canelli et al. 2012; Costa 1984; Takahashi 2014).

Observations of real debris flows show a great variability with regard to their physical parameters: velocities, mass fractions, and densities vary in part by several orders of magnitude. The range of observed velocities is from less than one m/s to more than 30 m/s, densities range from 1,130 to more than 2,500 kg/m<sup>3</sup> and solid volume fractions between 0.4 and 0.8 were observed. The average grain size diameter of natural debris flows ranges from 10<sup>-5</sup> to 10 m while flow heights vary from a few centimeters to more than 10 m (Costa 1984; Iverson 1997).

Owing to their high density in the range of up to more than twice the density of water and their high mobility, debris flows pose a significant threat to settlements, infrastructure, and human life (Fuchs et al. 2019; Hübl et al. 2009). To mitigate the risks that are associated with the highly variable debris-flow process, protective measures are employed. Their design requires models for debris-flow impact forces or pressures. According to Proske et al. (2011) and Suda et al. (2013), who studied debris-flow impact on breakers, debris-flow impact models consist of two parts: the process model and the impact model. The process model describes the behavior of the debris flow in the channel and the interaction between these components, respectively. Parameters from the process model such as density  $\rho$ , flow height  $h$ , and velocity  $v$  find their way into the abstracted impact model, which describes the impact of the debris flow on an obstacle. The impact model contains an estimate of

the peak debris-flow force  $F_{Peak}$  or the peak debris-flow pressure and the corresponding distribution (Fig. 3).

Common approaches for the estimation of debris-flow impact forces and pressures are usually divided in hydraulic (hydrostatic, hydrodynamic, and combined models), solid body collision, shock wave theory collision, and purely empirical models.

Hydraulic-hydrostatic models have been discussed in Armanini (1997), Hübl et al. (2009), and Lichtenhahn (1973). For those models, the debris-flow density and flow height are the factors governing debris-flow impact pressures. Hydraulic-hydrodynamic models are based on the assumption that the debris-flow velocity and flow type define debris-flow impact pressures. Examples can be found in Bugnion et al. (2012), Moriguchi et al. (2009), Watanabe and Ikeya (1981), and Zhang (1993) and hydraulic-combined models have been, for instance, examined by Arattano and Franzi (2003), Kherkheulidze (1969), Li et al. (2021), and Scheidl et al. (2023). These models assume, as the name suggests, that both static (flow height) and dynamic (flow velocity) elements are decisive for debris-flow impact pressures. Models for solid body collision are commonly built on the Hertz model, presuming elastic material behavior that is governed by the modulus of elasticity of the material. Examples can be found in Chen and Tang (2006), He et al. (2007), Lien (2002), Mizuyama (1979), VanDine (1996), and Yu and Tuan (2003), whereas shock wave theory-based models are discussed by Eglit et al. (2007) as well as Preece and Macmillan (1977). These models take the shock wave velocity inside a debris flow into account.

There has been a number of studies examining the impact forces of other processes on bridge superstructures; for example, tsunamis (Azadbakht and Yim 2015; Istrati et al. 2020, 2018), waves originating from hurricanes (Guo et al. 2015), and (woody) debris transport occurring in the course of floods (Fenske et al. 1995; Jempson 2000; Oudenbroek et al. 2018), yet debris-flow impact forces on bridge superstructures have not been analyzed so far.

Although it is essential to observe real debris flows and quantify their parameters due to the highly complex and variable character of the process, it is extremely difficult to carry out such observations. In addition to the high costs of large-scale measuring systems and the associated maintenance effort, the temporal and spatial prediction of debris-flow events is also nontrivial (Hübl et al. 2009). Laboratory experiments therefore are beneficial because they permit the production of controllable and monitorable debris flows to enable a detailed observation of the process.

In the past, many experiments have been conducted to analyze debris-flow impact on vertical obstacles that correspond to either bridge piers (Wang et al. 2018) or protection structures and abstract rigid vertical obstacles (Armanini et al. 2020, 2011; Cui et al. 2015;

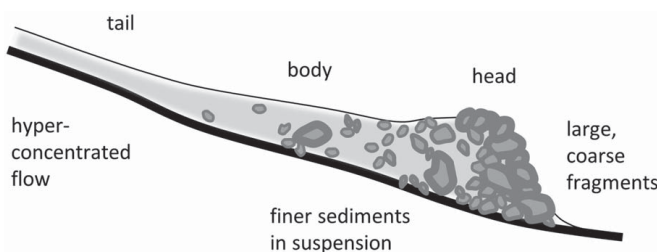


**Fig. 2.** Debris-flow architecture. (Reprinted with permission Taylor & Francis Ltd., *Hillslope Processes: Binghamton Geomorphology Symposium 16*, T. C. Pierson, “Flow behavior of channelized debris flows, Mount St. Helens, Washington,” © 2005, permission conveyed through Copyright Clearance Center, Inc.)

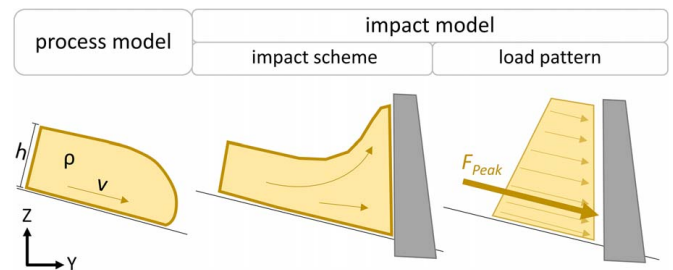


**Fig. 3.** Debris-flow process- and impact model. (“Debris flow impact estimation for breakers,” J. Suda, D. Proske, and J. Hübl, *Georisk: Assessment and Management of Risk for Engineered Systems and Geohazards*, © 2011, reprinted by permission of Taylor & Francis Ltd., <http://tandfonline.com>.)

Scheidl et al. 2023; Song et al. 2021; Vagnon and Segalini 2016) as well as flexible barriers or nets (Ashwood and Hungr 2016; Canelli et al. 2012; Ng et al. 2017; Wendeler and Volkwein 2015; Yifru et al. 2019). We assume that the acting forces on bridges and horizontal obstacles are not necessarily the same as for vertical barriers as the debris flow can pass under the superstructure, which is not the case for total impact. In addition, the geometrical conditions vary between the cases: the bridge superstructure covers only a small part of the total debris-flow height, while impacted vertical barriers are usually in a comparable dimension with the height of the debris flows.

Until now, there are no known experimental studies that have focused on debris-flow impact forces on bridge superstructures. All investigations carried out so far refer either to highly abstract and predominantly vertical obstacles (Armanini et al. 2020, 2011; Cui et al. 2015; Scheidl et al. 2023; Song et al. 2021; Vagnon and Segalini 2016; Wang et al. 2018) or to other flow processes (Azadbakht and Yim 2015; Fenske et al. 1995; Guo et al. 2015; Istrati et al. 2020, 2018; Jempson 2000; Oudenbroek et al. 2018) that are unarguably different from debris-flow events, as runoff behavior during floods is characterized by a longer duration with high discharge and can be described as almost stationary, while debris flow events are short and have transient characteristics.

The only known study on physical modeling of debris-flow impact on bridge superstructures (Proske et al. 2018) is based on a strong simplification when transferring the impact forces to the bridge. Proske et al. (2018) investigated debris-flow impact on masonry arch bridges, performing their experiments in two stages. In a first step, miniaturized debris-flow impact tests were carried out with a measuring body that was equipped with load cells. Based on these measurements, a significant impact force or stress was determined. In the second step, this dynamic horizontal impact load was applied to an arch bridge model at a scale of 1:2. During the test, the compression, displacements, and cracks on the arch were recorded. In the study at hand, however, we present the first systematic and combined analysis of debris-flow impact forces on bridge superstructures under consideration of different bridge profiles.

Research in this domain is highly relevant as it appears to be mandatory to design bridges to withstand such impacts, as documented events show that debris flows and their impact forces play a significant role in the failure of bridges and as there is evidence that the areas that are prone to debris-flow events may

increase in the future as a consequence of climate change (Schlögl et al. 2021). Until now, the mechanisms and consequences of debris-flow impact on bridge superstructures are unclear. From these considerations we identified the research gap and derived research questions to be answered in this paper: What forces occur on bridge superstructures during debris-flow impact? What is the influence of the bridge profile and of a bridge pier on these forces? How can the peak debris-flow force be related to the superstructure?

We aim to answer these questions by developing a load pattern for the described load case and by measuring and quantifying the impact forces on bridge superstructures using miniaturized laboratory experiments at a scale of 1:30. We will first describe the experimental setup and methodological background. We will then focus on the load pattern and finally present the results of the laboratory experiments with an emphasis on the effective frontal impact forces of the debris-flow. In addition, we will relate the data from our laboratory experiments to previously conducted experiments by Scheidl et al. (2023) and discuss our findings and their implications.

## Methodology

### Experimental Setup

The experimental setup used by Scheidl et al. (2023) was adapted to also include the instrumented miniature bridge profile. The flume (Fig. 4) consists of a 100 cm rectangular sheet metal stretch that is followed by a semicircular channel with a length of 400 cm and a diameter of 30 cm, part of which is covered with a roughness layer. The channel is framed by wooden formwork panels, and it is mounted on two 600 cm-long HEB steel beams. The channel's inclination is fixed at  $20^\circ$ , as this has been found to be the optimal slope for the development of a homogeneous (in terms of flow height and flow velocity) and reproducible granular experimental debris flow. A higher slope angle would come close to the natural internal friction angle of granular debris flows and therefore could lead to instabilities. A lower slope would impair the reproducibility of the experimental granular debris flow.

To reduce the influence of vibrations on the measurements, the whole construction is fixed to two concrete blocks. After being

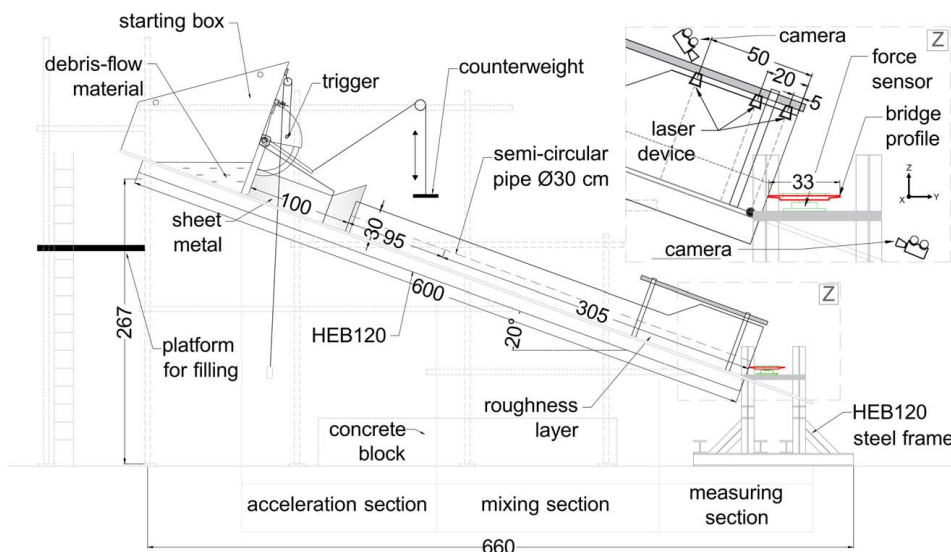


Fig. 4. Experimental setup, all measurements in cm.



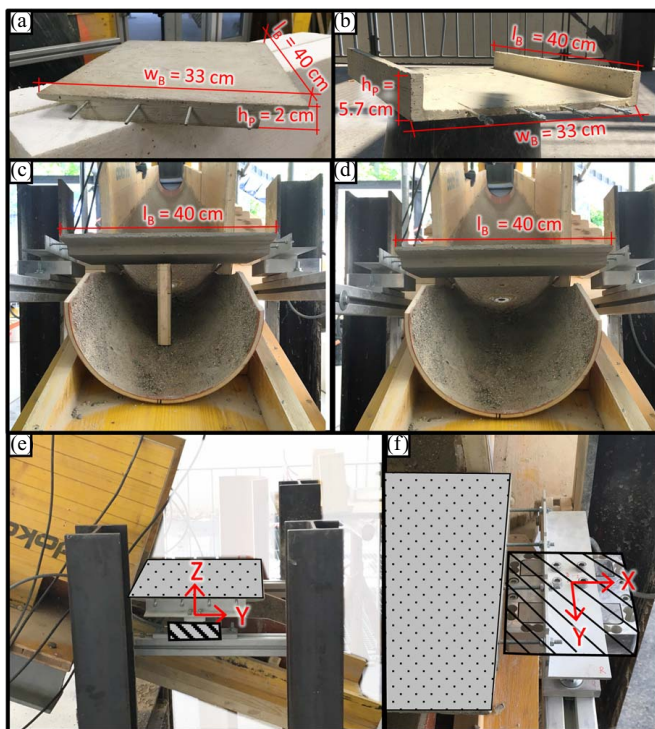
released from a rectangular starting box in a dam-break scenario, the debris-flow material forms a typical debris-flow-like habitus of the head–body–tail architecture (Pierson 2020) while travelling down the acceleration section and the mixing section. The debris flow then enters the measuring section before hitting the instrumented miniature bridge profile at the end of the flume (Fig. 5).

We chose to study six different bridge profiles that represent common types of Alpine bridges: the full slab, the broad beam, the box-girder, the trough, the T-beam and the slab profile (Fig. 6). Each profile has a length  $l_B$  of 40 cm normal to the direction of flow and a width  $w_B$  of 33 cm in the direction of the flow. The total height of the profiles  $h_P$  ranges from 1.3 to 5.7 cm [Figs. 5(a) and (b), Fig. 6]. All profiles are made of cement and plaster reinforcement [Figs. 5(a) and (b)]. The profiles are traversed by steel threaded rods that allow fixation on the force sensors [Figs. 5(a)–(d)], which are mounted on a HEB120-steel frame that is decoupled from the flume to avoid the influence of remaining vibrations of the channel. Each profile was mounted at the same height of 9.5 cm above the channel surface to ensure comparability of the setups. The removable bridge pier is made of wood and is not force-locked with the bridge profile as it is only intended to influence the flow behavior of the debris flow [Figs. 5(c) and (d)].







We conducted five replicates with and five replicates without the pier for each of the six profiles ( $i_{\text{set}} = 5$ ), resulting in a total of 60 experimental runs. However, during postprocessing, irregular process conditions had to be assumed for one replicate (#16, broad-beam profile with pier). Thus, a total of 59 experiments were used for further analyses.

### Debris-Flow Material

Natural debris flows show great variability in terms of their grain composition (Costa 1984; Iverson 1997). Taking this fact into



**Fig. 5.** (a) Full slab profile; (b) trough profile; (c) setup with pier; (d) setup without pier; (e) side view; and (f) top view of 3-axis force sensors (dashed) and bridge profile (dotted) with dimensions.

(a) Full slab  $h_P = 2.0 \text{ cm}$ $h_P^* = 0.60 \text{ m}$	(b) Broad beam  $h_P = 2.7 \text{ cm}$ $h_P^* = 0.81 \text{ m}$	(c) T-beam  $h_P = 3.3 \text{ cm}$ $h_P^* = 0.99 \text{ m}$
(d) Box-girder  $h_P = 4.2 \text{ cm}$ $h_P^* = 1.26 \text{ m}$	(e) Slab  $h_P = 1.3 \text{ cm}$ $h_P^* = 0.39 \text{ m}$	(f) Trough  $h_P = 5.7 \text{ cm}$ $h_P^* = 1.71 \text{ m}$

**Fig. 6.** Bridge profiles and dimensions in model ( $h_P$ ) and prototype ( $h_P^*$ ).

account is beyond the scope of this paper, therefore the debris-flow composition is based on previously conducted physical modeling of debris flows with natural material (D'Agostino et al. 2010; Scheidl et al. 2015, 2023). We used five different grain size classes of crushed stone, which were weighed and mixed to form the solid part of our bulk mixture. The total mass for each replicate was kept constant at 50 kg, of which 37.5 kg are solids and 12.5 kg are water. This corresponds to a solid–fluid ratio in terms of volume of 65:35%. The debris-flow density  $\rho$  is 1,920 kg/m<sup>3</sup>. To ensure reproducibility and to minimize unwanted and uncontrollable effects of changing water content in the debris flow, the material was mixed newly for each replicate—the material was not reused. The applied mixture, however, refers to the same granular debris flows as discussed in Scheidl et al. (2023), whose flow resistance is largely dominated by friction or collision conditions. These granular debris flows in the low Froude region are reasonably common, as reported in field observations (Costa 1984; Lapillonne et al. 2023; Zhou et al. 2019).

### Scaling Considerations

The requirement for a model to ensure similarity to a full-scale prototype or, in other words, to be able to transfer the model results to conditions in nature is compliance with geometric, kinematic, and dynamic similarity (Heller 2012). Geometric similarity is considered by the constant characteristic length scale  $\lambda$ , which represents the ratio of the prototype ( $l^*$ ) and laboratory ( $l$ ) length dimensions as

$$\lambda = \frac{l^*}{l} = 30 \quad (1)$$

Kinematic similarity between prototypical debris flows and our replicates is reached through the flume inclination, roughness of the bed, and choice of material.

Full dynamic similarity cannot be reached as long as the same fluid with the same viscosity as in nature is used in the tests (Iverson 1997). However, Froude similarity can be used to approximate dynamic similarity. As the experiments feature a free surface flow, inertial and gravitational forces outweigh frictional forces, and we therefore can apply the Froude scaling concept (Froude similarity). There is evidence to support the idea that experimental results can be accepted as long as Froude similarity is maintained (Vagnon and Segalini 2016).

Ranges of flow heights  $h$ , velocities  $v$ , Froude numbers  $Fr$ , and impact forces  $F_F$  from the laboratory experiments and the prototypical values  $h^*$ ,  $v^*$ , and  $F_F^*$  can be found in Table 1. The calculations were performed according to Heller (2012).

**Table 1.** Model ( $x$ ) and prototype ( $x^*$ ) parameters

Calculation Unit	Flow height $h\lambda = h^*$		Velocity $v\sqrt{\lambda} = v^*$		Froude number $Fr\lambda^0 = Fr^*$ $Fr(\lambda) = Fr^*(\lambda)$	Frontal impact force $F_F\lambda^3 = F_F^*$	
	$h$ (cm)	$h^*$ (m)	$v$ (m/s)	$v^*$ (m/s)		$F_F$ (N)	$F_F^*$ (kN)
Median	11.3	3.39	1.1	6.2	1.07	45.5	1,229
Std. Deviation	$\pm 1.0$	$\pm 0.29$	$\pm 0.2$	$\pm 1.0$	$\pm 0.18$	$\pm 18.9$	$\pm 510$

### Measurement Technique and Postprocessing

Two Actionpro X8 cameras were installed on the flume. The video material was solely used for visual assessment of the experiments.

All measurements were started simultaneously by a trigger that is integrated in the opening mechanism of the starting box and were stopped automatically after 30 s. Using Baumer OADM 2016480/S14F laser distance sensors, flow heights were measured at three locations in the flume. The flow velocity was calculated from the laser measurements based on the passage time of the debris-flow front between the sensors (Scheidl et al. 2013) and was solely used to calculate the Froude number  $Fr$ . The two 3-axis force sensors ME K3D120 are installed on either side of the miniature bridge at the bridge abutments to measure the impact forces [Figs. 5(e) and (f)].

A Quantum MX1601B datalogger from HBM was used to amplify the signals and the corresponding software Catman V5.3.2 was used for postprocessing. A sampling frequency of 2,400 Hz was chosen to safely ensure compliance with the Nyquist theorem. After reviewing the recorded data, all files were cut after 7 s, which corresponds to the passage time of the slowest debris flow. The Fast Fourier Transform of the raw impact force data showed a disturbance at 50 Hz, which supposedly originated from electrical equipment in the vicinity and therefore had to be removed from the signal before further analysis of the data. For this reason and to distinguish between impact of individual particles from impact of the bulk mass, on which this study focuses, the impact force data were further postprocessed with Python using a Butterworth-Lowpass filter with a cutoff frequency of  $f_c = 30$  Hz. The filter was chosen because of its steep step response in the frequency domain and the good stopband attenuation, whereas the cutoff frequency was chosen to match experimental debris flow impact studies with comparable scaling considerations (Baselt et al. 2021; Eu et al. 2019; Ng et al. 2017; Scheidl et al. 2013). The laser data were filtered with a median filter with a length of 241, which corresponds to 10% of the sampling frequency.

Because of the characteristics of the 3-axis force sensors and their arrangement, it was possible to measure one force value in each direction at any time during the test. For each replicate  $i$  and at each point in time  $t$ , we therefore obtained three force values from the right sensor and from the left sensor. To gain the resulting force per axis at each point in time and replicate, the values of the left and the right sensors were consequentially summed up. Thus, corresponding to Figs. 5(e) and (f), we define  $F_{Y,t,i}$  as the sum of horizontal forces,  $F_{Z,t,i}$  as the sum of vertical forces, and  $F_{X,t,i}$  as the sum of lateral forces of both sensors. However, since the lateral forces summed up close to zero,  $F_{X,t,i}$  is subsequently omitted.

We then calculated the effective frontal impact force for each replicate  $F_{F,i}$  from the force components in  $Y$ - and  $Z$ -direction  $F_{Y,i}$  and  $F_{Z,i}$  at each timestep, and set the maximum value of each experiment as

$$F_{F,i} = \sqrt{F_{Y,i}^2 + F_{Z,i}^2} \quad (2)$$

Because preliminary tests showed that surcharge of material on the bridge superimposed all force measurements, a special screen

was installed, preventing material from being deposited on the bridge. All processed data are listed in Appendix I.

### Idealized Load Pattern for Debris-Flow Impact on a Bridge Superstructure

To shed light on the question of the acting forces on bridge superstructures during debris-flow impact, we developed a load pattern (Fig. 7) based on findings from previous research (Fenske et al. 1995; Oudenbroek et al. 2018; Proske et al. 2018).

All acting forces are first assumed to be area loads. The multiplication of these loads by the length of bridge section that is exposed to the flow or, in the case of  $F_{Peak}$ , with the width of the channel, results in idealized line loads. These line loads are multiplied by the corresponding dimensions to obtain point loads that are indicated in Fig. 7.

We assume the pressure distribution of the total debris-flow impact (Fig. 3) to be the section force in the debris flow. The peak debris-flow force  $F_{Peak}$  is thus henceforth considered an internal process parameter. In our approach, the distribution of this load is assumed to be trapezoidal. Depending on the impact model used to determine this quantity, this distribution can also take other forms.

The idealized load pattern is composed of four force components, which will be described in the following. As the debris flow hits the bridge superstructure, the effective frontal impact force  $F_F$  is exerted by the frontal impact of the debris flow on the exposed face of the bridge superstructure. Owing to the inclination of the channel and the horizontal positioning of the bridge, this force consists of two components:  $F_Y$  and  $F_Z$  [Eq. (2)]. Depending on the characteristics of the bridge superstructure and the flow height of the debris flow, material may be deposited on top of the bridge, resulting in the surcharge load or force  $F_{Top}$ . In principle, it is further conceivable that in certain configurations of bridge form and inclination of the channel, the flowing debris flow may touch the underside of the bridge and thereby induce a horizontal frictional force  $F_{Fric}$  and a force in the upward direction  $F_{Up}$  that consists of uplift and/or buoyancy forces.

Since the possibility of an additional surcharge was eliminated through shielding in all experiments,  $F_{Top}$  can be assumed to be

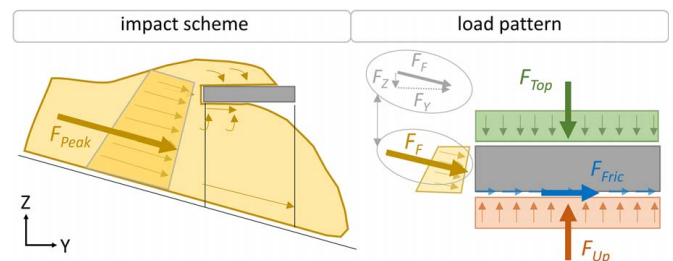


**Fig. 7.** Theoretical impact scheme and load pattern for debris-flow impact on a bridge superstructure. For illustration purposes, the effective frontal impact force  $F_F$  is parallel to the channel bottom. Note that the direction of  $F_F$  can also be upward.

zero in this study. Furthermore, the idealized point loads,  $F_{\text{Fric}}$  as well as  $F_{\text{Up}}$ , could not be detected in any of the conducted experiments. The videos of the experiments rather suggest that there is no contact of the experimental debris flow with the underside of the bridge model. In this study, we use the measurements from the laboratory experiments to examine the effective frontal impact force  $F_F$  of the load pattern in more detail.

## Results

### Influence of the Bridge Superstructure Profiles and Bridge Pier on Magnitude and Direction of the Effective Frontal Impact Force $F_F$

To compare and investigate the influence of the different bridge superstructure profiles with and without piers, we normalized the individual  $F_{F,i}$ -values by the mean of all replicates  $i$ , resulting in a dimensionless factor  $\mu_{F,i}$ , which can be represented as

$$\mu_{F,i} = F_{F,i} / \left( \frac{\sum_{i=1}^{59} F_{F,i}}{59} \right) \quad (3)$$

We further assume that the impact of a debris flow on an obstacle can possibly also be characterized by an arbitrary direction of the effective frontal impact force. For this reason, we also estimated the direction of the effective frontal impact force, given by the impact angle  $\beta_i$  as

$$\beta_i = \text{atan} \left( \frac{F_{Z,i}}{F_{Y,i}} \right) \quad (4)$$

While a positive impact angle  $\beta_i$  indicates a positive (upward) vertical frontal force component  $F_Z$ , a negative impact angle  $\beta_i$  means that the vertical force component  $F_Z$  is negative respectively downward orientated.

In Fig. 8, distributions of  $\mu_{F,i}$  and  $\beta_i$  clustered according to profile and pier criterion are compared. Here, increasing  $\beta_i$  at same  $\mu_{F,i}$  values mean a larger absolute vertical force component  $F_Z$  in relation to the horizontal force component  $F_Y$ . Conversely, the smaller the angle  $\beta_i$  the more dominant  $F_Y$  gets:  $\beta_i = \pm 45^\circ$  means that the absolute values of  $F_Y$  and  $F_Z$  are equally large, while an angle of  $\beta_i = \pm 5^\circ$  indicates that  $F_Z$  is only slightly under 10% of the magnitude of  $F_Y$ . Since most values of  $\beta_i$  lie in the range of  $\pm 5^\circ$ , it follows that the contribution of the vertical component  $F_Z$  on the magnitude of the effective frontal impact force is not particularly pronounced.

Our results show highest effective frontal impact forces for the bridge profiles box-girder and trough and lowest for the slab bridge profile, for both with and without pier configuration. A clear trend

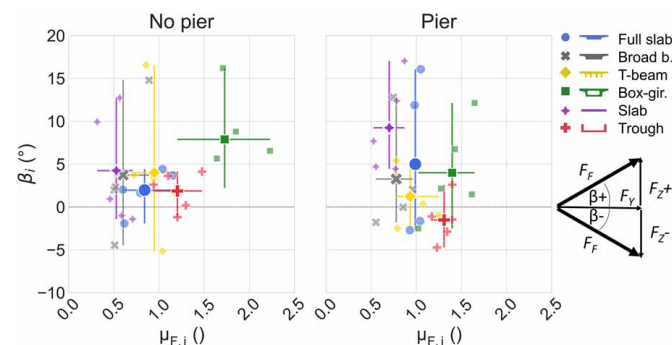


Fig. 8. Scatterplots of mean  $F_{F,i}$  and  $\beta_i$  per setup with ranges.

regarding the influence of the pier on the direction of the effective frontal impact force cannot be discerned from the results, as most of the angles of impact are positive (upward oriented). Only for the trough bridge profile a negative (downward oriented) impact angle can be observed. However, our results suggest that the presence of a pier means that the influence of the different bridge superstructures on the effective frontal impact force  $F_F$  is less widely dispersed.

### Influence of Profile and Pier on the Horizontal Impact Force $F_Y$ and the Vertical Impact Force $F_Z$

To study the influence of the pier and the profiles on the horizontal component of the effective frontal impact force, we normalized  $F_{Y,i}$  by the mean of all replicates to obtain the dimensionless related factor  $\mu_{Y,i}$ , which can be presented as

$$\mu_{Y,i} = F_{Y,i} / \left( \frac{\sum_{i=1}^{59} F_{Y,i}}{59} \right) \quad (5)$$

The same procedure was followed for the vertical component, and a similar procedure was followed to derive the dimensionless related factor  $\mu_{Z,i}$  using

$$\mu_{Z,i} = F_{Z,i} / \left( \frac{\sum_{i=1}^{59} F_{Z,i}}{59} \right) \quad (6)$$

Fig. 9 shows distributions of  $\mu_{Y,i}$  for each bridge profile, one with and one without pier. Here the lowest horizontal impact forces, that is, lowest  $\mu_{Y,i}$  values, can be observed for the slab profile, while the box-girder profile is responsible for the largest measured horizontal impact forces, corresponding to highest  $\mu_{Y,i}$  values.

Fig. 9 indicates that the different bridge profiles do have an influence on the magnitude of the related horizontal impact forces. This is confirmed by a one-way ANOVA that resulted in a rejection of the null hypothesis based on a  $P$ -value below 0.001 at a significance level of  $\alpha = 0.05$ . However, to find out which profiles do have a similar influence on the horizontal forces that occur, we performed a Tukey's honestly significant difference (HSD) test for equality of means over multiple treatments, comparing the profile groups in a pairwise fashion (Table 2).

Tukey's HSD test showed that the impact influence of the Full slab, Broad beam and T-beam profiles do not differ significantly from each other. The results also show that the Slab profile is clearly different from all other profiles, except for the Broad

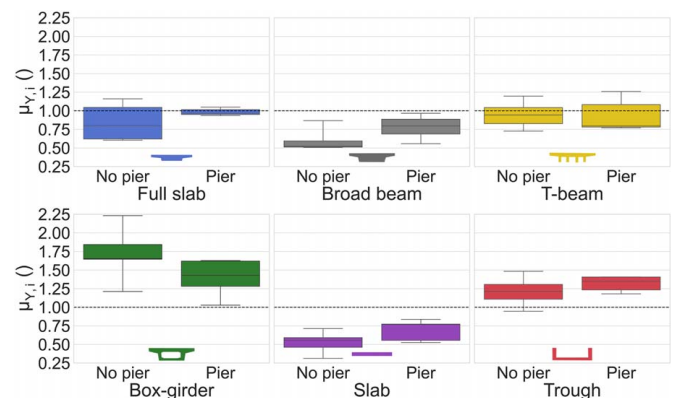


Fig. 9. Boxplots of  $\mu_{Y,i}$ .



**Table 2.** Results of Tukey's HSD test

Group 1	Group 2	$F_Y$		$F_Z$	
		P-value	Reject <sup>a</sup>	P-value	Reject <sup>a</sup>
Full slab	Broad beam	0.19	No	0.9	No
Full slab	T-beam	0.9	No	0.9	No
Full slab	Box-girder	0.001	Yes	0.15	No
Full slab	Slab	0.03	Yes	0.9	No
Full slab	Trough	0.01	Yes	0.79	No
Broad beam	T-beam	0.11	No	0.9	No
Broad beam	Box-girder	0.001	Yes	0.1	No
Broad beam	Slab	0.9	No	0.9	No
Broad beam	Trough	0.001	Yes	0.9	No
T-beam	Box-girder	0.001	Yes	0.04	Yes
T-beam	Slab	0.02	Yes	0.9	No
T-beam	Trough	0.02	Yes	0.9	No
Box-girder	Slab	0.001	Yes	0.26	No
Box-girder	Trough	0.03	Yes	0.01	Yes
Slab	Trough	0.001	Yes	0.62	No

<sup>a</sup>Based on  $\alpha = 0.05$ .

beam profile. All other profile pairings show significant differences regarding the horizontal impact force  $F_Y$ .

To analyze the influence of the pier on the magnitude of the horizontal impact force for each bridge profile, we further performed an independent two-sample  $t$ -test, testing the differences between the setup with and without pier at a significance level of  $\alpha = 0.05$ . Our results show that the null hypothesis could not be rejected for any profile (Table 3), which means that the pier has no significant influence on the magnitude of the horizontal impact force  $F_Y$ .

Fig. 10 shows distributions of  $\mu_{Z,i}$  for each bridge profile, once with and without pier. The absolute values of the vertical force component are small, as the consideration of the impact angle showed. Therefore, while the absolute variation of the measured forces is low (Appendix I), the relative variation of  $\mu_{Z,i}$  is large. The Tukey's HSD test indicated no significant difference of the values between the profile groups with the exception of the pairings box-girder and T-beam profile as well as the Box-girder and Trough-profile (Table 2). The  $t$ -test for the influence of the pier also shows no significant differences for the vertical component, with the exception of the Slab profile (Table 3). Since the forces  $F_{Z,i}$  are rather small, we do not consider this to be relevant for further investigations.

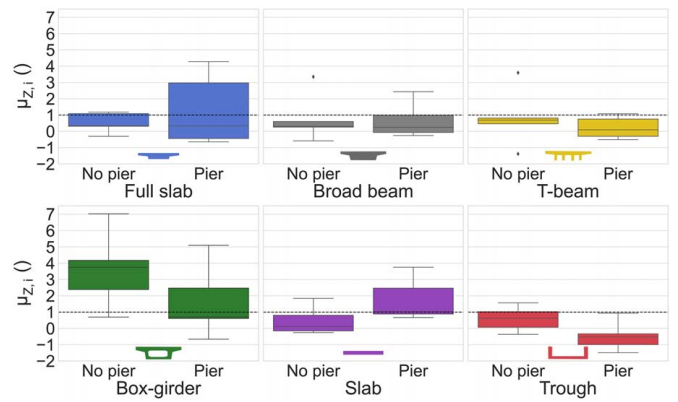
### Relation of Effective Frontal Impact Force $F_F$ and Peak Debris-Flow Force $F_{Peak}$

Since the usual approach to the design of protective measures against debris flows refer to the peak pressure or peak force (Fig. 3) (Hübl et al. 2017), we established a relationship between the peak debris-flow force  $F_{Peak}$  and the effective frontal impact force  $F_F$  exerted and measured on the bridge. This is important

**Table 3.** Results of  $t$ -test for significant influence of the pier

Name	$F_Y$		$F_Z$	
	P-value	Reject <sup>a</sup>	P-value	Reject <sup>a</sup>
Full slab	0.29	No	0.48	No
Broad beam	0.16	No	0.44	No
T-beam	0.94	No	0.42	No
Box-girder	0.15	No	0.71	No
Slab	0.11	No	0.03	Yes
Trough	0.35	No	0.39	No

<sup>a</sup>Based on  $\alpha = 0.05$ .

**Fig. 10.** Boxplots of  $\mu_{Z,i}$ .

as we assume that the acting forces on bridges and horizontal obstacles, respectively, are not necessarily the same as for vertical obstacles in the flow.

Values for the peak debris-flow force  $F_{Peak}$  originate from the experiments of Scheidl et al. (2023). In their study, debris-flow impact tests were carried out on a rigid and instrumented vertical obstacle. Because their experiments were conducted based on the same scaling considerations, with the same mixture in the same experimental flume used for this study and their experiments lay within a Froude region comparable to ours, we assume those values to be transferable to our results. Based on the same filtering procedure as described in this study, we processed the raw impact force data of all ten granular replicates conducted by Scheidl et al. (2023). However, because the flow velocity and subsequently the impact force of replicate #1 were low in comparison to all other replicates, it was discarded as an outlier for this study. In total, peak debris-flow forces  $F_{Peak}$  of  $n = 9$  replicates could thus be used for further analyses. Appendix II contains the data applied in this study.

The effective frontal impact force acting on the bridge superstructure in relation to the expected peak debris-flow force of the considered debris flow is then given by

$$\mu_{i,n} = F_{F,i} / F_{Peak,n} \quad (7)$$

In Eq. (7),  $\mu_{i,n}$  is referred to as effective force coefficient and is defined as the quotient of each effective frontal impact force  $F_{F,i}$  divided by each of the  $n = 9$  peak debris-flow forces  $F_{Peak,n}$  as derived from experiments of (Scheidl et al. 2023). This results in a total of 45 values per setup, as  $i_{Set} = 5$ . The mean effective force coefficient  $\mu$  is calculated for each setup.

A dimensionless height ratio, denoted as effective height coefficient  $\eta_{eff,i}$  is given by

$$\eta_{eff,i} = h_p / h_i \quad (8)$$

The effective height coefficient  $\eta_{eff,i}$  [Eq. (8)] represents the ratio between the superstructure height  $h_p$  of the given bridge profile (Fig. 6) and the respective flow height  $h_i$  of the debris-flow replicate. Thus,  $\eta_{eff,i}$  accounts for both the variable phenomenological characteristic of the process in the form of the flow height and the different construction heights of the bridge profiles. The mean effective height coefficient  $\eta_{eff}$  is calculated for each setup.

Fig. 11 relates the mean effective force coefficient  $\mu$  for each bridge profile, with and without pier, to the corresponding mean effective height coefficient  $\eta_{eff}$  and additionally contains the ranges of all values of  $\mu_{i,n}$  and  $\eta_{eff,i}$ .

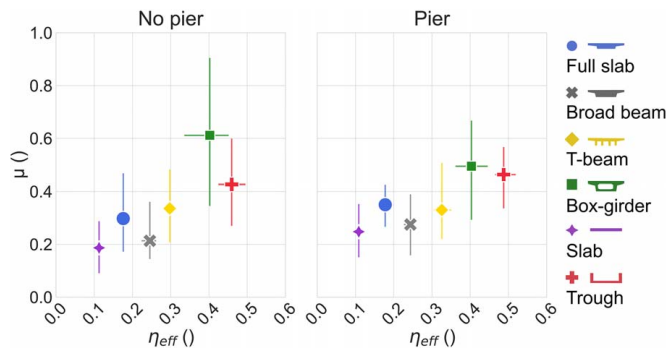


**Fig. 11.** Average values of  $\mu$  and  $\eta_{\text{eff}}$  per setup with ranges.

The mean values of the effective impact coefficients  $\mu$  are lowest for the slab profile and highest for the box-girder. The same is approximately true for the mean effective height coefficient  $\eta_{\text{eff}}$ , where the lowest values can be observed for the slab profile and the highest values refer to trough and box-girder profiles, respectively. Thus, bridge profiles with higher effective height coefficients also show higher effective force coefficients.

## Discussion

Bridge failures due to natural hazard processes are often attributed to hydrodynamic forces and loading by debris, that is, loading by any floating material. While existing studies consider the effects of hydrodynamic forces and debris drift on bridges (Fenske et al. 1995; Oudenbroek et al. 2018), there is a lack of information on the effects of debris-flow impact on bridge superstructures, where “debris” is understood to be the main component of the flowing mixture. However, the proposed idealized load pattern for debris flows impacting a bridge superstructure is based on concepts for hydrodynamic force effects and consists of four forces that act independently: an effective frontal impact force  $F_F$ , a surcharge force  $F_{\text{Top}}$ , a horizontal friction force  $F_{\text{Fric}}$ , and an uplift or buoyancy force  $F_{\text{Up}}$  (Fig. 7).

Preliminary tests in our experimental setup, in which effective frontal impact forces  $F_F$  and surcharge forces  $F_{\text{Top}}$  were shielded, showed that neither horizontal friction forces  $F_{\text{Fric}}$  nor uplift forces  $F_{\text{Up}}$  could be detected. Further, an analysis of the video footage of all conducted experiments revealed that the underside of the bridge model appeared dry after the tests, indicating no contact with the debris-flow material at all. The bridge model was not subjected to horizontal frictional forces or uplift forces, and it is therefore plausible that no transmission of forces to the underside of the bridge took place in our tests. We attribute this to the steep slope of the channel, which leads to a rapid increase in the potential freeboard or distance between the channel bottom and the underside of the bridge. This seems plausible, because debris flows, especially those of a granular nature, mainly form in channel with slopes ranging roughly from  $13^\circ$  up to  $30^\circ$  (Rickenmann 2016). However, debris-flow properties depend not only on the slope but also on the flow resistance and the channel geometry (Iverson 1997; Jakob and Hungr 2005). Therefore, the occurrence of horizontal friction forces and uplift forces acting on bridge superstructures cannot be excluded for debris flows characterized by different rheological or geometrical conditions from the prototypical settings used in this study. In practical conditions, debris-flow material might be deposited on the bridge superstructure, leading to a surcharge force  $F_{\text{Top}}$ . Preliminary tests in our study showed that this surcharge force superimposes any other measurements in the

vertical direction. We therefore shielded the superstructure from material deposition, consciously neglecting the surcharge force  $F_{\text{Top}}$  in this study.

For granular debris flows, the effective frontal impact force  $F_F$  appears to be the most significant load case regarding bridge superstructures. However, the angle of impact of the effective frontal impact force  $\beta$  does not seem to be consistent. We expected  $F_F$  to act in the same direction as the inclination of the flume, which corresponds to  $20^\circ$ , but our results show that for most of the replicates the direction of the  $F_F$  component in the  $Z$ -direction is upward (Fig. 8). We assume that the debris mass is compressed and pushed upward by the cross-sectional constriction during impact, thus changing the direction of the vertical force component of  $F_F$ . This can also be seen to some extent in the influence of the pier, which increases the mean impact angles  $\beta$ , while at the same time equalizing the influence of the different profiles on  $F_F$ . However, apart from the box-girder profile without pier and the slab profile with pier, all mean values of  $\beta$  range from  $-5^\circ$  to  $+5^\circ$ . The largest part of the effective frontal impact force is therefore transferred horizontally to the superstructure, while the vertical component usually accounts for  $<10\%$ .

The horizontal component of the effective frontal impact force  $F_Y$  seems to depend on the bridge superstructure profile (Fig. 9, Table 2), and subsequently on the total height of the profile  $h_p$ . An increasing magnitude of the horizontal impact force  $F_Y$  can be observed with the increasing total height of the profile  $h_p$ . This observation is true for all profiles except the broad beam, which cannot be explained in this framework. The pier does not influence the magnitude of  $F_Y$  significantly, which might be attributable to the fact that the pier is not force-locked with the superstructure and to its placement behind the face of the superstructure (Table 3). The vertical component  $F_Z$  does not seem to depend on the bridge superstructure profile (Fig. 10, Table 2).

It can usually be expected that only part of the debris-flow induced peak load impacting a vertical obstacle can be attributed to the effective frontal impact force transferred on a bridge superstructure. For this study, we define the proportion of the peak debris-flow force  $F_{\text{Peak}}$  that is transferred to the bridge superstructure as the effective impact coefficient  $\mu$ , which can be back-calculated if  $F_{\text{Peak}}$  is known. To date, however, there is no generally valid debris-flow impact model, and the number of studies modeling the effects of peak debris-flow force  $F_{\text{Peak}}$  is steadily increasing (Armanini et al. 2020; Calvetti et al. 2016; Eu et al. 2019; Huang and Zhang 2022; Ng et al. 2021; Tang and Hu 2018; Vagnon and Segalini 2016). The reason for the multitude of studies is the different observable dynamic behavior of debris flows, which is proportional to its destructive power. The determination of input variables to estimate plausible peak debris-flow impact forces is therefore complex and must be decided in practice on a case-by-case basis. For this reason, we applied  $F_{\text{Peak}}$  values that were determined in the course of comparable laboratory experiments (Scheidt et al. 2023). The analysis shows that most back-calculated effective impact coefficients  $\mu$  lay below 0.5, which indicates that  $<50\%$  of the debris-flow peak force effectively impacts the superstructures of bridges (Fig. 11). Higher effective impact coefficients have only been detected for the box-girder profile without pier configuration. However, this profile type also shows the greatest fluctuations.

Relating the effective impact coefficient  $\mu$  with the effective height coefficient  $\eta_{\text{eff}}$  provides the possibility to estimate the expected impact forces on a bridge superstructure and thus to design resilient bridge structures for the load case under consideration, being particularly relevant in areas endangered by frequently occurring debris flows.



Limits of our study result mainly from the fact that our experimental debris flows are consciously focused on a single material mix and that the slope of the flume is held constant. Furthermore, all profiles were installed at the same height above the channel bottom, which was established with regard to the experimental flow heights. For future investigations and to extend the validity of the results, it would be of interest to investigate other material mixtures, channel slopes, and installation heights of the bridges as well as the remaining components of the theoretical load pattern  $F_{Fric}$ ,  $F_{Up}$ , and  $F_{Top}$  that have not been addressed in this study. Owing to the complex process of debris flow, it can be assumed that the change of the mentioned parameters will provide new insights.

## Conclusions

Previous studies on the impact forces of debris flows refer either to quite abstract or mainly vertical obstacles. Therefore, experimental studies that take a holistic approach to analyzing impact forces of debris flows on bridge superstructures, especially beam bridges, are both innovative and unique. We found that the choice of the bridge profile influences the magnitude of the effective frontal impact forces and that the presence or absence of a bridge pier affects the direction of the effective frontal impact force, but not necessarily its magnitude. We related the total debris-flow force determined from previous experiments to the bridge superstructure by calculating a dimensionless coefficient that varies depending on the profile. We showed that the forces that act on bridge superstructures are on average between one- and three-fifths of the total debris-flow force, depending on the profile. We have also shown that the effective frontal impact force acts mainly in the horizontal direction, the vertical proportion is mostly < 10%. These findings can contribute to a better design of bridges against debris-flow impact in the future.

Our small-scale laboratory experiments have laid the foundation for further detailed examination of debris-flow impact on bridge superstructures. Future research may include the investigation of other material mixtures, channel slopes and bridge installation heights.

## Appendix I. Compiled Processed Data of Bridge Superstructure Replicates

#	Profile	Pier	$h$ (cm)	$F_F$ (N)	$F_Y$ (N)	$F_Z$ (N)	$\beta$ (°)
1	Full slab	no	11.9	29.8	29.8	-1.0	-1.92
2	Full slab	no	10.6	29.0	29.0	1.0	2.02
3	Full slab	no	11.9	50.3	50.1	3.9	4.43
4	Full slab	no	11.4	38.3	38.3	1.1	1.65
5	Full slab	no	11.2	55.8	55.6	3.6	3.69
6	Full slab	yes	11.0	50.7	48.7	14.0	16.07
7	Full slab	yes	12.1	50.3	50.3	-1.4	-1.63
8	Full slab	yes	12.0	45.6	45.6	1.1	1.39
9	Full slab	yes	11.4	44.9	44.8	-2.1	-2.70
10	Full slab	yes	10.1	47.4	46.4	9.8	11.88
11	Broad beam	no	11.0	24.3	24.3	0.8	1.99
12	Broad beam	no	10.3	25.1	25.1	1.0	2.33
13	Broad beam	no	10.8	28.6	28.5	2.0	3.97
14	Broad beam	no	12.1	24.6	24.5	-1.9	-4.46
15	Broad beam	no	11.0	43.0	41.6	11.0	14.79
16	Broad beam	yes	12.3	26.8	22.8	-14.0	-31.49
17	Broad beam	yes	10.6	36.0	35.1	8.0	12.81
18	Broad beam	yes	11.2	41.3	41.3	0.0	-0.02
19	Broad beam	yes	10.7	26.7	26.7	-0.8	-1.79
20	Broad beam	yes	11.9	46.4	46.3	1.7	2.06
21	Box-girder	no	9.3	58.2	58.2	2.3	2.24

(Continued.)

#	Profile	Pier	$h$ (cm)	$F_F$ (N)	$F_Y$ (N)	$F_Z$ (N)	$\beta$ (°)
22	Box-girder	no	11.0	89.5	88.4	13.7	8.80
23	Box-girder	no	10.6	79.3	78.9	7.8	5.66
24	Box-girder	no	9.4	107.8	107.1	12.3	6.56
25	Box-girder	no	12.5	82.6	79.3	23.0	16.20
26	Box-girder	yes	9.7	49.4	49.3	-2.2	-2.51
27	Box-girder	yes	11.6	69.0	68.6	8.1	6.75
28	Box-girder	yes	11.3	61.5	61.5	2.3	2.15
29	Box-girder	yes	9.4	79.5	77.7	16.7	12.13
30	Box-girder	yes	10.4	78.1	78.0	2.0	1.47
31	Trough	no	11.5	45.4	45.4	2.1	2.60
32	Trough	no	13.0	71.4	71.2	5.1	4.13
33	Trough	no	13.4	58.2	58.2	-1.2	-1.18
34	Trough	no	11.8	62.7	62.7	0.2	0.20
35	Trough	no	12.5	53.3	53.2	3.4	3.62
36	Trough	yes	11.5	67.5	67.5	3.1	2.60
37	Trough	yes	11.0	64.8	64.7	-3.3	-2.88
38	Trough	yes	11.9	67.5	67.5	-1.7	-1.46
39	Trough	yes	11.9	56.6	56.6	-1.1	-1.10
40	Trough	yes	12.3	59.4	59.2	-4.9	-4.72
41	T-Beam	no	10.7	41.4	39.6	11.8	16.56
42	T-Beam	no	11.4	57.4	57.4	1.5	1.52
43	T-Beam	no	10.5	45.3	45.2	2.7	3.39
44	T-Beam	no	11.6	34.9	34.9	2.3	3.73
45	T-Beam	no	11.3	50.2	50.0	-4.5	-5.17
46	T-Beam	yes	10.8	37.0	36.9	2.5	3.84
47	T-Beam	yes	10.3	37.6	37.5	3.5	5.40
48	T-Beam	yes	10.1	38.3	38.3	-1.7	-2.49
49	T-Beam	yes	9.4	51.9	51.9	0.3	0.34
50	T-Beam	yes	10.0	60.4	60.4	-1.0	-0.93
51	Slab	no	11.5	15.3	15.0	2.6	9.94
52	Slab	no	10.9	22.2	22.2	0.4	0.94
53	Slab	no	12.3	28.4	28.4	-0.5	-1.00
54	Slab	no	12.6	34.2	34.2	-0.8	-1.41
55	Slab	no	10.7	27.4	26.7	6.0	12.74
56	Slab	yes	12.0	26.7	26.6	2.2	4.69
57	Slab	yes	11.2	37.8	36.9	8.1	12.39
58	Slab	yes	11.3	37.2	37.1	2.9	4.45
59	Slab	yes	14.2	42.0	40.2	12.3	17.03
60	Slab	yes	11.7	25.4	25.2	3.4	7.68

## Appendix II. Compiled Processed Data of Force Plate Panel Replicates

Exp. Nr.	$F_{Peak}$ (N)
1	86.2
2	119.1
3	125.2
4	125.7
5	142.0
6	132.1
7	135.3
8	140.9
9	168.3
10	152.4

Source: Data from Scheidl et al. (2023).

## Data Availability Statement

The raw and filtered data as well as the code that support the findings of this study are available from the corresponding author upon reasonable request.

## Acknowledgments

This study was conducted as part of the project Nr. P 32511 “Debris-flow impact forces on bridge superstructures” funded by the Austrian Science Fund (FWF). The experiments were conducted at the Institute of Mountain Risk Engineering (IAN) at the University of Natural Resources and Life Sciences, Vienna. We thank Ing. Friedrich Zott for his support in the laboratory.

## Notation

The following symbols are used in this paper:

- $F_F$  = effective frontal impact force (N, kN);  
 $F_{F,i}$  = effective frontal impact force from measurements per replicate (N);  
 $F_{Fric}$  = frictional force (N, kN);  
 $F_{Peak}$  = peak debris-flow force (N, kN);  
 $F_{Peak,n}$  = peak debris-flow force of Scheidl et al. (2023) (N);  
 $F_F^*$  = effective frontal impact force—prototype (kN);  
 $Fr$  = Froude number;  
 $Fr^*$  = Froude number of prototype;  
 $F_{Top}$  = surcharge force (N, kN);  
 $F_{Up}$  = uplift and/or buoyancy force (N, kN);  
 $F_{x,t,b}$ ,  $F_{y,t,b}$ ,  $F_{z,t,i}$  = sum of measured forces over time per replicate (N);  
 $F_Y$  = horizontal force component of effective frontal impact force (N, kN);  
 $F_{Y,i}$  = measured horizontal force component of  $F_{F,i}$  (N);  
 $F_Z$  = vertical force component of effective frontal impact force (N, kN);  
 $F_{Z,i}$  = measured vertical force component of  $F_{F,i}$  (N);  
 $f_c$  = cutoff frequency of Butterworth-lowpass filter (30 Hz);  
 $h$ ,  $h_i$  = flow height of debris flow, per replicate (cm, m);  
 $h^*$  = flow height of debris flow—prototype (m);  
 $h_p$  = height of bridge model (mm);  
 $h_p^*$  = height of bridge profile—prototype (m);  
 $i$  = replicate;  
 $i_{Set}$  = number of replicates per setup (5);  
 $l^*$  = prototype dimension;  
 $l$  = model dimension;  
 $l_b$  = length of bridge model (mm);  
 $n$  = replicate of (Scheidl et al. 2023);  
 $v$  = velocity of debris flow (m/s);  
 $v^*$  = velocity of debris flow—prototype (m/s);  
 $w_b$  = width of bridge model (cm);  
 $\beta_i$  = impact angle per replicate ( $^\circ$ );  
 $\eta_{eff}$  = effective height coefficient per setup;  
 $\eta_{eff,i}$  = effective height coefficient per replicate;  
 $\lambda$  = characteristic length scale;  
 $\mu$  = effective force coefficient for forces on bridge superstructures per setup;  
 $\mu_{i,n}$  = effective force coefficient for forces on bridge superstructures per replicate;  
 $\mu_F$ ,  $\mu_{F,i}$  = factor for frontal impact forces, per replicate;  
 $\mu_Y$ ,  $\mu_{Y,i}$  = factor for horizontal component of frontal impact forces, per replicate; and  
 $\rho$  = density of debris flow ( $\text{kg/m}^3$ ).

## References

- Arattano, M., and L. Franzi. 2003. “On the evaluation of debris flows dynamics by means of mathematical models.” *Nat. Hazards Earth Syst. Sci.* 3: 539–544. <https://doi.org/10.5194/nhess-3-539-2003>.
- Armanini, A. 1997. “On the dynamic impact of debris flows.” In *Recent developments on debris flows*, edited by A. Armanini, and M. Michiue, 208–226. Berlin: Springer.
- Armanini, A., M. Larcher, and M. Odorizzi. 2011. “Dynamic impact of a debris flow front against a vertical wall.” *Ital. J. Eng. Geol. Environ.* 1041–1049. <https://doi.org/10.4408/IJEGE.2011-03.B-113>.
- Armanini, A., G. Rossi, and M. Larcher. 2020. “Dynamic impact of a water and sediments surge against a rigid wall.” *J. Hydraul. Res.* 58: 314–325. <https://doi.org/10.1080/00221686.2019.1579113>.
- Ashwood, W., and O. Hungr. 2016. “Estimating total resisting force in flexible barrier impacted by a granular avalanche using physical and numerical modeling.” *Can. Geotech. J.* 53: 1700–1717. <https://doi.org/10.1139/cgj-2015-0481>.
- Azadbakht, M., and S. C. Yim. 2015. “Simulation and estimation of tsunami loads on bridge superstructures.” *J. Waterw. Port Coastal Ocean Eng.* 141: 04014031. [https://doi.org/10.1061/\(ASCE\)WW.1943-5460.0000262](https://doi.org/10.1061/(ASCE)WW.1943-5460.0000262).
- Baselt, I., G. Queiroz De Oliveira, J.-T. Fischer, and S. P. Pudasaini. 2021. “Evolution of stony debris flows in laboratory experiments.” *Geomorphology* 372: 107431. <https://doi.org/10.1016/j.geomorph.2020.107431>.
- Bugnion, L., B. W. McArdell, P. Bartelt, and C. Wendeler. 2012. “Measurements of hillslope debris flow impact pressure on obstacles.” *Landslides* 9: 179–187. <https://doi.org/10.1007/s10346-011-0294-4>.
- Calvetti, F., C. di Prisco, and E. Vairaktaris. 2016. “Dry granular flows impacts on rigid obstacles: DEM evaluation of a design formula for the impact force.” *Procedia Eng.* 158: 290–295. <https://doi.org/10.1016/j.proeng.2016.08.444>.
- Canelli, L., A. M. Ferrero, M. Migliazza, and A. Segalini. 2012. “Debris flow risk mitigation by the means of rigid and flexible barriers – experimental tests and impact analysis.” *Nat. Hazards Earth Syst. Sci.* 12: 1693–1699. <https://doi.org/10.5194/nhess-12-1693-2012>.
- Chen, H. K., and H. M. Tang. 2006. “Method to calculate impact force and impact time of two-phase debris flow.” *Chin. J. Highw. Transp.* 19: 19–23.
- Chiarle, M., S. Iannotti, G. Mortara, and P. Deline. 2007. “Recent debris flow occurrences associated with glaciers in the Alps.” *Global Planet. Change* 56: 123–136. <https://doi.org/10.1016/j.gloplacha.2006.07.003>.
- Costa, J. E. 1984. “Physical geomorphology of debris flows.” In *Developments and applications of geomorphology*, edited by J. E. Costa, and P. J. Fleisher, 268–317. Berlin: Springer.
- Cui, P., C. Zeng, and Y. Lei. 2015. “Experimental analysis on the impact force of viscous debris flow.” *Earth Surf. Processes Landforms* 40: 1644–1655. <https://doi.org/10.1002/esp.3744>.
- D’Agostino, V., M. Cesca, and L. Marchi. 2010. “Field and laboratory investigations of runout distances of debris flows in the Dolomites (Eastern Italian Alps).” *Geomorphology* 115: 294–304. <https://doi.org/10.1016/j.geomorph.2009.06.032>.
- Eglit, M. E., V. S. Kulibaba, and M. Naaim. 2007. “Impact of a snow avalanche against an obstacle. Formation of shock waves.” *Cold Reg. Sci. Technol.* 50: 86–96. <https://doi.org/10.1016/j.coldregions.2007.06.005>.
- Eu, S., S. Im, and D. Kim. 2019. “Development of debris flow impact force models based on flume experiments for design criteria of soil erosion control dam.” *Adv. Civ. Eng.* 2019: 1–8. <https://doi.org/10.1155/2019/3567374>.
- Fan, X., et al. 2019. “Earthquake-induced chains of geologic hazards: Patterns, mechanisms, and impacts.” *Rev. Geophys.* 57: 421–503. <https://doi.org/10.1029/2018RG000626>.
- Fenske, T., C. Apelt, and A. Parola. 1995. *Debris forces and impact on highway bridges* (No. 73/1/73/2). Zurich, Switzerland: IABSE.
- Fuchs, S., M. Keiler, R. Ortler, R. Schinke, and M. Papatoma-Köhle. 2019. “Recent advances in vulnerability assessment for the built environment exposed to torrential hazards: Challenges and the way forward.” *J. Hydrol.* 575: 587–595. <https://doi.org/10.1016/j.jhydrol.2019.05.067>.

- Guo, A., Q. Fang, X. Bai, and H. Li. 2015. "Hydrodynamic experiment of the wave force acting on the superstructures of coastal bridges." *J. Bridge Eng.* 20: 04015012. [https://doi.org/10.1061/\(ASCE\)BE.1943-5592.0000758](https://doi.org/10.1061/(ASCE)BE.1943-5592.0000758).
- He, S. M., X. P. Li, and Y. Wu. 2007. "Calculation of impact force of out-runner blocks in debris flow considering elastoplastic deformation." *Chin. J. Rock Mech. Eng.* 26: 1664–1669.
- Heller, V. 2012. "Development of wave devices from initial conception to commercial demonstration." *Compr. Renewable Energy* 8: 79–110. <https://doi.org/10.1016/B978-0-08-087872-0.00804-0>.
- Huang, Y., and B. Zhang. 2022. "Challenges and perspectives in designing engineering structures against debris-flow disaster." *Eur. J. Environ. Civ. Eng.* 26: 4476–4497. <https://doi.org/10.1080/19648189.2020.1854126>.
- Hübl, J., G. Nagl, J. Suda, and F. Rudolf-Miklau. 2017. "Standardized stress model for design of torrential barriers under impact by debris flow (according to Austrian standard regulation 24801)." *Int. J. Erosion Control Eng.* 10: 47–55. <https://doi.org/10.13101/ijece.10.47>.
- Hübl, J., J. Suda, D. Proske, R. Kaitna, and C. Scheidl. 2009. "Debris flow impact estimation." In *Proc., 11th Int. Symp. on Water Management and Hydraulic Engineering*, edited by C. Popovska and M. Jovanovski, 137–148. Skopje, Macedonia: University of Ss.
- Istrati, D., I. Buckle, P. Lomonaco, and S. Yim. 2018. "Deciphering the tsunami wave impact and associated connection forces in open-girder coastal bridges." *J. Mar. Sci. Eng.* 6: 148. <https://doi.org/10.3390/jmse6040148>.
- Istrati, D., A. Hasanpour, and I. Buckle. 2020. "Numerical investigation of tsunami-borne debris damming loads on a coastal bridge." In *Proc., 17th World Conf. on Earthquake Engineering*. Sendai, Japan: Japan Association for Earthquake Engineering.
- Iverson, R. M. 1997. "The physics of debris flows." *Rev. Geophys.* 35: 245–296. <https://doi.org/10.1029/97RG00426>.
- Iverson, R. M. 2000. "Landslide triggering by rain infiltration." *Water Resour. Res.* 36: 1897–1910. <https://doi.org/10.1029/2000WR900090>.
- Jakob, M., and O. Hungr. 2005. *Debris-flow hazards and related phenomena*. Berlin: Springer.
- Jempson, M. A. 2000. "Hydrodynamic forces on partially and fully submerged bridge superstructures." *Ph.D. thesis. School of Engineering, Univ. of Queensland*.
- Kherkheulidze, I. 1969. "Estimation of basic characteristics of mudflow ('sel')." In *Proc., of the Leningrad Symp. on Floods and Their Computation*, 940–948. Leningrad, Russia: IASH-Unesco-WMO.
- Lapillonne, S., F. Fontaine, F. Liebault, V. Richefeu, and G. Piton. 2023. "Debris-flow surges of a very active alpine torrent: A field database." *Nat. Hazards Earth Syst. Sci.* 23: 1241–1256. <https://doi.org/10.5194/nhess-23-1241-2023>.
- Li, X., J. Zhao, and K. Soga. 2021. "A new physically based impact model for debris flow." *Géotechnique* 71: 674–685. <https://doi.org/10.1680/jgeot.18.P.365>.
- Lichtenhahn, C. 1973. "Die berechnung von sperren in beton und eisenbeton." In *Kolloquium Über wildbachsperren*, 91–127. Vienna, Austria: Österr. Agrarverl.
- Lien, H. P. 2002. "Study on treatment of debris flow (II)." Taiwan: Soil and Water Conservation Bureau, Council of Agriculture (COA).
- Mizuyama, T. 1979. "Computational method and some considerations on impulsive force of debris flow acting on Sabo Dams." *J. Jpn. Soc. Eros. Control Eng.* 112: 40–43.
- Moriguchi, S., R. I. Borja, A. Yashima, and K. Sawada. 2009. "Estimating the impact force generated by granular flow on a rigid obstruction." *Acta Geotech.* 4: 57–71. <https://doi.org/10.1007/s11440-009-0084-5>.
- Mostbauer, K., R. Kaitna, D. Prenner, and M. Hrachowitz. 2018. "The temporally varying roles of rainfall, snowmelt and soil moisture for debris flow initiation in a snow-dominated system." *Hydrol. Earth Syst. Sci.* 22: 3493–3513. <https://doi.org/10.5194/hess-22-3493-2018>.
- Ng, C. W. W., H. Liu, C. E. Choi, J. S. H. Kwan, and W. K. Pun. 2021. "Impact dynamics of boulder-enriched debris flow on a rigid barrier." *J. Geotech. Geoenviron. Eng.* 147: 04021004. [https://doi.org/10.1061/\(ASCE\)GT.1943-5606.0002485](https://doi.org/10.1061/(ASCE)GT.1943-5606.0002485).
- Ng, C. W. W., D. Song, C. E. Choi, L. H. D. Liu, J. S. H. Kwan, R. C. H. Koo, and W. K. Pun. 2017. "Impact mechanisms of granular and viscous flows on rigid and flexible barriers." *Can. Geotech. J.* 54: 188–206. <https://doi.org/10.1139/cgj-2016-0128>.
- OEBB-Infrastruktur AG. 2022. *ÖBB infra zahlen-daten-fakten*. Vienna, Austria: OEBB-Infrastruktur AG.
- Oudenbroek, K., N. Naderi, J. Bricker, Y. Yang, C. van der Veen, W. Uijtewaal, S. Moriguchi, and S. Jonkman. 2018. "Hydrodynamic and debris-damming failure of bridge decks and piers in steady flow." *Geosciences* 8: 409. <https://doi.org/10.3390/geosciences8110409>.
- Pierson, T. C. 2020. "Flow behavior of channelized debris flows, Mount St. Helens, Washington." In *Hillslope processes*, edited by A. D. Abrahams, 269–296. London: Routledge. (Original work published 1986).
- Preece, C. M., and N. H. Macmillan. 1977. "Erosion." *Annu. Rev. Mater. Sci.* 7: 95–121. <https://doi.org/10.1146/annurev.ms.07.080177.000523>.
- Prenner, D., M. Hrachowitz, and R. Kaitna. 2019. "Trigger characteristics of torrential flows from high to low alpine regions in Austria." *Sci. Total Environ.* 658: 958–972. <https://doi.org/10.1016/j.scitotenv.2018.12.206>.
- Proske, D., A. Krawtschuk, O. Zeman, C. Scheidl, and M. Chiari. 2018. "Debris flow impacts on masonry arch bridges." *Proc. Inst. Civ. Eng. Bridge Eng.* 171: 25–36. <https://doi.org/10.1680/jbren.16.00005>.
- Proske, D., J.-B. Payeur, B. Girardin, and H. Friedl. 2022. "Risk based maintenance for Swiss railway bridges: Concept, implementation and first experiences." *Acta Polytech. CTU Proc.* 36: 167–174. <https://doi.org/10.14311/APP.2022.36.0167>.
- Proske, D., J. Suda, and J. Hübl. 2011. "Debris flow impact estimation for breakers." *Georisk: Assess. Manage. Risk Eng. Syst. Geohazards* 5: 143–155. <https://doi.org/10.1080/17499518.2010.516227>.
- Rickenmann, D. 2016. *Methods for the quantitative assessment of channel processes in torrents (steep streams)*. 1st ed. IAHR Monographs. London: CRC Press.
- SBB AG. 2022. *SBB-CFF-FFS Zahlen und Fakten 2021*. Bern, Switzerland: SBB AG.
- Scheidl, C., M. Chiari, R. Kaitna, M. Müllegger, A. Krawtschuk, T. Zimmermann, and D. Proske. 2013. "Analysing debris-flow impact models, based on a small scale modelling approach." *Surv. Geophys.* 34: 121–140. <https://doi.org/10.1007/s10712-012-9199-6>.
- Scheidl, C., C. Friedl, L. Reider, S. Wernhart, A.-L. Fuchs, A. L. Dankwerth, G. Nagl, R. Kaitna, and D. Proske. 2023. "Impact dynamics of granular debris flows based on a small-scale physical model." *Acta Geotech.* <https://doi.org/10.1007/s11440-023-02116-8>.
- Scheidl, C., B. W. McArdeell, and D. Rickenmann. 2015. "Debris-flow velocities and superelevation in a curved laboratory channel." *Can. Geotech. J.* 52: 305–317. <https://doi.org/10.1139/cgj-2014-0081>.
- Schlögl, M., S. Fuchs, C. Scheidl, and M. Heiser. 2021. "Trends in torrential flooding in the Austrian Alps: A combination of climate change, exposure dynamics, and mitigation measures." *Clim. Risk Manage.* 32: 100294. <https://doi.org/10.1016/j.crm.2021.100294>.
- Song, D., X. Chen, G. G. D. Zhou, X. Lu, G. Cheng, and Q. Chen. 2021. "Impact dynamics of debris flow against rigid obstacle in laboratory experiments." *Eng. Geol.* 291: 106211. <https://doi.org/10.1016/j.enggeo.2021.106211>.
- Suda, J., J. Hübl, and F. Rudolf-Miklau. 2013. "Standardisiertes einwirkungsmodell zur bemessung von wildbachsperren unter mureinwirkung." *Bautechnik* 90: 792–802. <https://doi.org/10.1002/bate.201300064>.
- Takahashi, T. 2014. *Debris flow: Mechanics, prediction, and countermeasures*. 2nd ed. Boca Raton, FL: CRC Press.
- Tang, J.-B., and K.-H. Hu. 2018. "A debris-flow impact pressure model combining material characteristics and flow dynamic parameters." *J. Mountain Sci.* 15: 2721–2729. <https://doi.org/10.1007/s11629-018-5114-z>.
- Vagnon, F., and A. Segalini. 2016. "Debris flow impact estimation on a rigid barrier." *Nat. Hazards Earth Syst. Sci.* 16: 1691–1697. <https://doi.org/10.5194/nhess-16-1691-2016>.
- VanDine, D. F. 1996. *Debris flow control structures for forest engineering (working paper)*, ministry of forests research program. Victoria, BC: Ministry of Forest Research Program.



- Wang, D., Z. Chen, S. He, Y. Liu, and H. Tang. 2018. "Measuring and estimating the impact pressure of debris flows on bridge piers based on large-scale laboratory experiments." *Landslides* 15: 1331–1345. <https://doi.org/10.1007/s10346-018-0944-x>.
- Watanabe, M., and H. Ikeya. 1981. "Investigation and analysis of volcanic mud flows on Mount Sakurajima, Japan." In *Proc., Florence Symp.*, 245–256. Florence, Italy: IAHS.
- Wendeler, C., and A. Volkwein. 2015. "Laboratory tests for the optimization of mesh size for flexible debris-flow barriers." *Nat. Hazards Earth Syst. Sci.* 15: 2597–2604. <https://doi.org/10.5194/nhess-15-2597-2015>.
- Yifru, A. L., H. Vicari, S. Nordal, and V. Thakur. 2019. "Laboratory investigation of the impact force of debris flow on a passable structure." In *Proc., 17 European Conf. on Soil Mechanics and Geotechnical Engineering*, edited by H. Sigursteinsson, S. Erlingsson, and B. Bessason, 2961–2968. Reykjavik, Iceland: The Icelandic Geotechnical Society (IGS).
- Yu, C. P., and C. H. Tuan. 2003. "On the impact responses of retaining structures due to massive rock debris flows and analytical approaches." *J. Chin. Soil Water Conserv.* 34: 55–66.
- Zhang, S. 1993. "A comprehensive approach to the observation and prevention of debris flows in China." *Nat. Hazard.* 7: 1–23. <https://doi.org/10.1007/BF00595676>.
- Zhou, G. G. D., H. S. Hu, D. Song, T. Zhao, and X. Q. Chen. 2019. "Experimental study on the regulation function of slit dam against debris flows." *Landslides* 16: 75–90. <https://doi.org/10.1007/s10346-018-1065-2>.